Journal of Solid State Chemistry 182 (2009) 3412–3415

Contents lists available at ScienceDirect

Journal of Solid State Chemistry

journal homepage: www.elsevier.com/locate/jssc

Rapid Communication

On the solid solution of the spinel phase in the system NiO–Al_2O_3

Magnus Rotan [a], Julian Tolchard [a], Erling Rytter [b], Mari-Ann Einarsrud [a], Tor Grande [a,*]

[a] Department of Materials Science and Engineering, Norwegian University of Science and Technology, NO-7491 Trondheim, Norway
[b] StatoilHydro, Research Centre, NO-7005 Trondheim, Norway

ARTICLE INFO

Article history:
Received 2 June 2009
Received in revised form
29 September 2009
Accepted 2 October 2009
Available online 8 October 2009

Keywords:
Solid solution
Spinel
$NiAl_2O_4$
X-ray diffraction

ABSTRACT

The solid solubility of Al_2O_3 in $NiAl_2O_4$ spinel has been investigated by powder X-ray diffraction of samples prepared by solid state synthesis. The solid solution region found was in agreement with a previous report. The cubic cell parameter of the spinel solid solution was observed to decrease with increasing alumina content. Spinel with high alumina content was shown to be close to an inverse spinel as previously reported for stoichiometric $NiAl_2O_4$ and the inversion parameter proved to be relatively independent of the overall composition.

1. Introduction

The formation of spinel phase is well known in binary oxide systems of alumina and divalent oxides (M=Mg or transition metals). The stoichiometric spinel phase has the formula MAl_2O_4, but non-stoichiometric spinels are also well known due to their extended solubility of Al_2O_3 [1–3]. In normal spinels the small M^{2+} ion is situated in tetrahedral sites and Al^{3+} in octahedral positions in the cubic closed packing of oxygen anions, while in inverse spinels the M^{2+} is located in octahedral positions and the Al^{3+} ions is located at both octahedral and tetrahedral positions. Intermediate spinels have cation arrangement intermediate between normal and inverse spinels. $NiAl_2O_4$ has a cation arrangement close to an inverse spinel at ambient temperature. The cations in $NiAl_2O_4$ have also been shown to approach random distribution with increasing temperature [4–10].

In this communication, we report on the solid solution of Al_2O_3 in $NiAl_2O_4$. The solid solubility of Al_2O_3 in $NiAl_2O_4$ has previously been reported, but no structural characterisation of the solid solutions has been reported. Here, we use Rietveld refinement of the diffraction data to determine the lattice parameter, cation site occupancy and atomic positions as a function of the alumina content in the spinel solid solution.

2. Experimental

2.1. Powder synthesis

Nine samples of nickel aluminate with different stoichiometry were synthesised via solid state reaction. NiO (Sigma-Aldrich, 99%) and γ-alumina (Merck, 99%) were pre-heated at 600 °C for 6 h and mixed in an agate mortar using acetone as mixing aid. Ethyl cellulose was added (~3 wt%) during the mixing as a binder for the subsequent isostatic dry pressing of the powder into 25 mm disks. The samples (~3 g) were placed on alumina disk supports and annealed three times in air at 1400 °C for 24 h in a chamber furnace. Each heating period was interspersed with regrinding, examination by X-ray powder diffraction and re-pressing into pellets. After the synthesis the samples were also equilibrated at two different temperatures, 800 and 1300 °C. The samples annealed at 1300 °C for 12 h (Q1300) were quenched to room temperature, while the samples annealed at 800 °C (C800) were cooled to ambient temperature by 300 °C/h. Previous reports have shown that the inversion parameter for the spinel is kinetically frozen in around 800 °C, while at 1300 °C a lower degree of inversion can be obtained by quenching the sample [8]. Trends in the distribution of Ni and Al between the two lattice sites in the spinel phase could therefore be obtained by these two sets of samples. The X-ray data obtained directly after the synthesis were relatively close to the ones obtained for the C800 series, but these are not reported due to a less defined thermal history.

2.2. Powder X-ray diffraction

Powder X-ray diffraction (XRD) data were collected on a Bruker AXS D8 Focus diffractometer with a Lynxeye™ detector using

* Corresponding author.
E-mail address: tor.grande@material.ntnu.no (T. Grande).

0022-4596/$ - see front matter © 2009 Elsevier Inc. All rights reserved.
doi:10.1016/j.jssc.2009.10.001

Table 1
Structural model for the spinel phase including the numerical expression for the occupancy of Ni^{2+}, Al^{3+} and vacancies used in the Rietveld refinement where x_{NiO} is the overall mol fraction of NiO.

Space group	Site	Np	x	y	z	Atom	Occupation	Temp. factors
$Fd\bar{3}m$	S_1	8	$=\frac{1}{4}$	$=\frac{1}{4}$	$=\frac{1}{4}$	Ni^{2+}	$=\frac{4}{(3-2x_{NiO})}x_{NiO}-2^*a$	Tet
						Al^{3+}	$=\left(\frac{4}{(3-2x_{NiO})}2(1-x_{NiO})-2\right)+2^*a+2^*b$	Tet
						Vacancy	$=\frac{4}{(3-2x_{NiO})}\left(\frac{1}{4}-\frac{x_{NiO}}{2}\right)-2^*b$	Tet
	S_2	16	$=\frac{5}{8}$	$=\frac{5}{8}$	$=\frac{5}{8}$	Al^{3+}	$=1-a-b$	Oct
						Ni^{2+}	a	Oct
						Vacancy	b	Oct
	S_3	32	u	u	u	O	1	Ox

The occupancies are refined by the parameters a and b.

Cu$K\alpha$ radiation accelerated at 40 kV and 40 mA, scanning in the 2θ range from 15° to 110° with a step size of 0.01° and a 0.35 s counting time at each step. The XRD data were refined using Bruker AXS′ Topas v2.1 refinement software. The background was modelled using a Chebychev polynomial and a Pearson type VII profile was used to describe the Bragg reflections. In the non-stoichiometric spinel, a model containing cation vacancies was introduced to compensate for the increasing alumina content. The model used for the occupancy and distribution of species on the octahedral and tetrahedral sites in the non-stoichiometric samples is given in Table 1. A hydrogen atom was used to represent a vacant site in the structure model. For the samples containing two phases the total site occupancies were constrained to the composition corresponding to the solid solution limit for alumina. Assuming no vacancies at the oxygen lattice the occupations of Ni^{2+}, Al^{3+} and vacancies on the tetrahedral and octahedral sites can be expressed as a function of the mol fraction of NiO, x_{NiO} (see Table 1).

As shown in Table 1, the cations and vacancies were distributed between tetrahedral and octahedral sites using a and b as refinement parameters. In total 23 independent variables were used in the refinement. The temperature factors were refined separately for the three atomic positions.

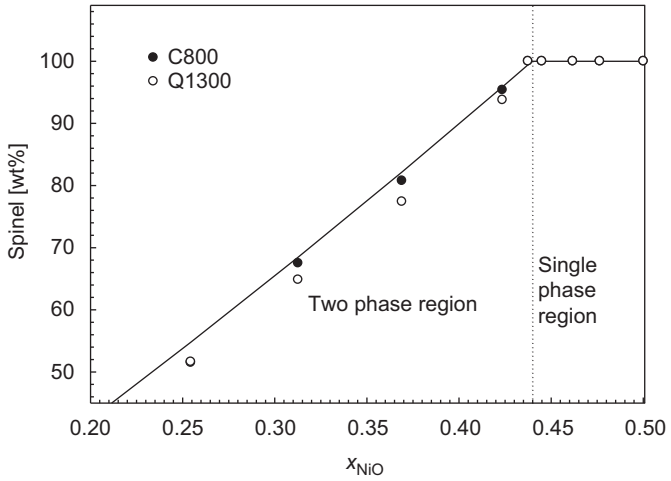

Fig. 1. The amount of spinel phase versus the overall composition of the samples. The statistical uncertainty in the refinement is within the size of the symbols.

3. Results and discussion

The phase composition of the samples found by XRD is shown in Fig. 1. The boundary for the single phase region was $x_{NiO}=0.44\pm0.01$, in relatively good agreement with a previous study [3]. Precipitation of a-alumina, in samples containing only spinel after the synthesis at 1400 °C was not observed after annealing at 800 °C. The temperature dependence of the solid solubility limit is therefore not very significant in line with the previous report. Elrefaie and Smeltzer found that the solubility limit was $x_{NiO}=0.42$ at 1400 °C by electron microprobe analysis. Similar measurements to elucidate possible loss of NiO in our samples due evaporation of NiO could not be performed due to the porous and fragile nature of the samples.

The refined lattice parameters for the nickel aluminate spinel for the different compositions are given in Table 2, and are plotted as a function of the overall composition in Fig. 2. The cubic lattice constant decreases linearly with increasing Al_2O_3 content in the single phase region. The cell parameter was significantly different for the C800 and Q1300 samples, demonstrating the influence of the temperature dependence of the inversion parameter. In the two phase region the spinel is saturated with alumina and one would expect the lattice parameter to become constant as shown by the dashed lines (Fig. 2). However, the parameters display a small increase with increasing alumina content. We propose that this is caused by the mismatch in thermal expansion between the two phases and that the spinel is put in tension during cooling of the samples. The increase in strain for decreasing values of x_{NiO} is explained by the increase in alumina crystallites in contact with each spinel crystallite. As an internal standard the lattice parameters for the α-alumina in the two phase region was also calculated and found to be unaltered and consistent with literature data [11]. The difference in strain can be explained by the much higher Young's modulus of the alpha alumina compared to the nickel aluminate [11,12]. The effect is also more pronounced for Q1300 samples than for C800 and this is evident due to the higher quenching temperature and the much shorter relaxation time for the Q1300 sample. The insert in Fig. 2 shows a linear regression of the lattice constant versus composition which coincides with the lattice constant for γ-alumina of 7.905 Å reported by Viertels et al. [13].

The lattice parameters for the Q1300 samples are in general higher than for the C800 samples. This can be understood from the change in the distribution of the cations at higher temperatures, see Fig. 3. The lattice constant for the different compositions is displayed as a function of temperature in Fig. 3. For all compositions the lattice parameter increases with increasing annealing temperature and the effect increases with increasing x_{NiO}. The data are in good accordance with what has been reported for stoichiometric $NiAl_2O_4$ [8,9].

Table 2
Lattice parameters for the spinel phase in the C800 and Q1300 samples.

wt% NiO	x_{NiO}	Lattice parameter (Å) C800	R_{wp}	Lattice parameter (Å) Q1300	R_{wp}
42.30	0.500	8.0457(2)	3.981	8.0513(2)	3.918
40.00	0.477	8.0364(2)	3.802	8.0405(2)	3.830
38.60	0.462	8.0308(2)	3.929	8.0336(3)	3.905
37.00	0.445	8.0283(3)	3.764	8.0316(3)	3.680
36.30	0.438	8.0274(3)	3.894	8.0281(4)	3.965
35.00	0.424	8.0272(4)	3.739	8.0295(3)	3.888
30.00	0.369	8.0281(3)	3.837	8.0322(2)	3.964
25.00	0.313	8.0283(2)	4.079	8.0333(2)	4.208
20.00	0.254	8.0309(1)	4.414	8.0338(2)	4.567

The R_{wp} is the sum of least squares of the difference between the refined and observed XRD patterns.

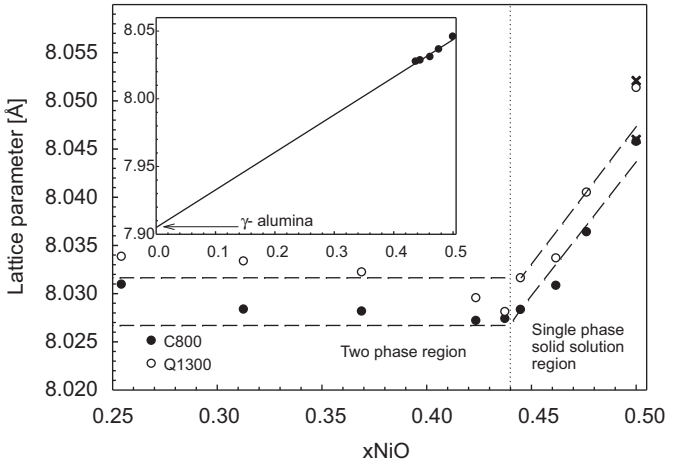

Fig. 2. Refined lattice parameters for $Ni_{1-x-y}Al_{2+x}\square_yO_4$ annealed at 800 and 1300 °C. Lattice parameters for stoichiometric spinel given by O'Neill et al. from quenched 800 and 1300 °C samples are included [8]. Insert: linear regression of the lattice parameter versus composition compared to the lattice parameter for γ-Al_2O_3 [12].

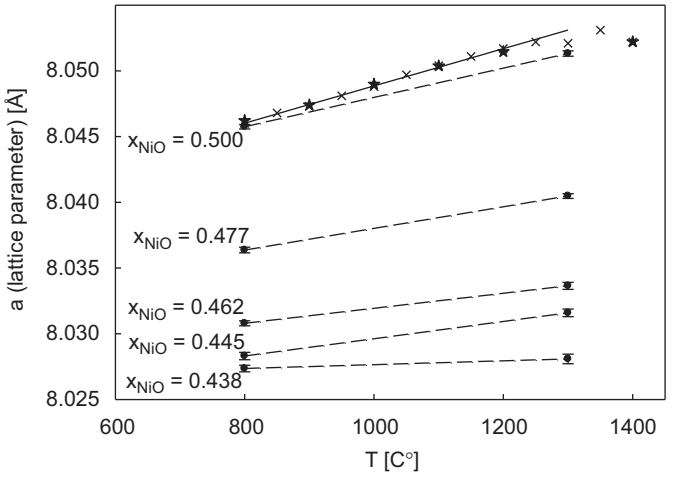

Fig. 3. The lattice parameter as a function of annealing temperature for five different compositions in the Al_2O_3–$NiAl_2O_4$ solid solution region. Literature data for stoichiometric spinel are included ×: O'Neill et al. [8], *: Roelofsen et al. [9].

The distribution of nickel between octahedral and tetrahedral positions in the spinel lattice as a function of the overall composition is given in Table 2 and shown in Fig. 4. The figure displays a decreasing trend for nickel in both positions for

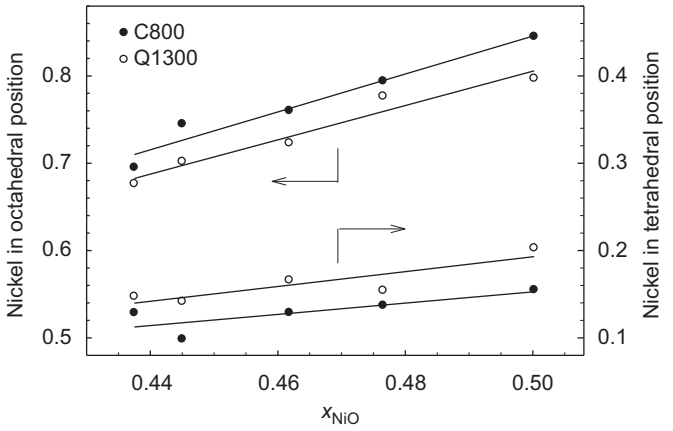

Fig. 4. The distribution of nickel between the octahedral and tetrahedral sites in the Al_2O_3–$NiAl_2O_4$ solid solution spinel. The numbers are pr. formula unit.

decreasing x_{NiO} and it follows that the inversion parameter defined as $Ni_{oct}/(Ni_{oct}+Ni_{tet})$ for all x_{NiO} becomes constant and is essentially independent of the overall composition. The inversion parameter found for $NiAl_2O_4$ at 800 and 1300 °C is in good accordance with previous reports [8,9]. The average inversion parameter for the solid solutions was 0.86 ± 0.01 and 0.82 ± 0.02 for C800 and Q1300, respectively. A higher preference of Ni for octahedral coordination for C800 than for Q1300 means that the inversion parameter decreases with increasing temperature which is in accordance with earlier observations [8,9]. The distribution of Ni, Al and vacancies on the two lattice sites is summarised in Table 3.

The oxygen parameter, which describes the deviations of the anions from the ideal fcc structure, versus the composition is shown in Fig. 5. In the single phase region the oxygen parameter for the C800 samples decreases with decreasing mol fraction of NiO and becomes constant when entering the two phase region. No clear trends are observed for the Q1300 samples. The relatively large scatter in the date reflects the weak contribution of oxygen to the Brag reflections.

4. Conclusion

Extensive solid solubility of α-Al_2O_3 in $NiAl_2O_4$ has been demonstrated. The unit cell parameter of the non-stoichiometric spinel phase was shown to decrease with increasing alumina content. The degree of inversion of the spinel solid solutions were not shown to depend strongly on the Al_2O_3 content. The solid solutions were close to an inverse spinel at low temperatures and

Table 3
The refined occupations pr formula unit of the spinel in the samples with nominal Ni content x_{NiO}.

x_{NiO}	C800	Q1300
0.500	$[Ni_{0.155}Al_{0.845}Vac_{0.000}]^{tet}[Ni_{0.845}Al_{1.155}Vac_{0.000}]^{oct}O_4$	$[Ni_{0.203}Al_{0.797}Vac_{0.000}]^{tet}[Ni_{0.797}Al_{1.203}Vac_{0.000}]^{oct}O_4$
0.477	$[Ni_{0.137}Al_{0.842}Vac_{0.021}]^{tet}[Ni_{0.794}Al_{1.204}Vac_{0.002}]^{oct}O_4$	$[Ni_{0.154}Al_{0.830}Vac_{0.016}]^{tet}[Ni_{0.777}Al_{1.216}Vac_{0.007}]^{oct}O_4$
0.462	$[Ni_{0.129}Al_{0.858}Vac_{0.014}]^{tet}[Ni_{0.760}Al_{1.216}Vac_{0.024}]^{oct}O_4$	$[Ni_{0.166}Al_{0.797}Vac_{0.037}]^{tet}[Ni_{0.732}Al_{1.277}Vac_{0.000}]^{oct}O_4$
0.445	$[Ni_{0.099}Al_{0.902}Vac_{0.000}]^{tet}[Ni_{0.745}Al_{1.201}Vac_{0.054}]^{oct}O_4$	$[Ni_{0.142}Al_{0.838}Vac_{0.020}]^{tet}[Ni_{0.702}Al_{1.266}Vac_{0.032}]^{oct}O_4$
0.438	$[Ni_{0.129}Al_{0.829}Vac_{0.042}]^{tet}[Ni_{0.695}Al_{1.288}Vac_{0.017}]^{oct}O_4$	$[Ni_{0.147}Al_{0.827}Vac_{0.026}]^{tet}[Ni_{0.676}Al_{1.290}Vac_{0.033}]^{oct}O_4$
0.424	$[Ni_{0.122}Al_{0.842}Vac_{0.037}]^{tet}[Ni_{0.702}Al_{1.276}Vac_{0.022}]^{oct}O_4$	$[Ni_{0.166}Al_{0.788}Vac_{0.047}]^{tet}[Ni_{0.658}Al_{1.330}Vac_{0.012}]^{oct}O_4$
0.369	$[Ni_{0.114}Al_{0.854}Vac_{0.032}]^{tet}[Ni_{0.710}Al_{1.264}Vac_{0.027}]^{oct}O_4$	$[Ni_{0.155}Al_{0.800}Vac_{0.044}]^{tet}[Ni_{0.668}Al_{1.317}Vac_{0.015}]^{oct}O_4$
0.313	$[Ni_{0.114}Al_{0.864}Vac_{0.022}]^{tet}[Ni_{0.709}Al_{1.254}Vac_{0.037}]^{oct}O_4$	$[Ni_{0.132}Al_{0.859}Vac_{0.009}]^{tet}[Ni_{0.692}Al_{1.258}Vac_{0.050}]^{oct}O_4$
0.254	$[Ni_{0.099}Al_{0.886}Vac_{0.016}]^{tet}[Ni_{0.725}Al_{1.232}Vac_{0.043}]^{oct}O_4$	$[Ni_{0.151}Al_{0.814}Vac_{0.035}]^{tet}[Ni_{0.673}Al_{1.303}Vac_{0.024}]^{oct}O_4$

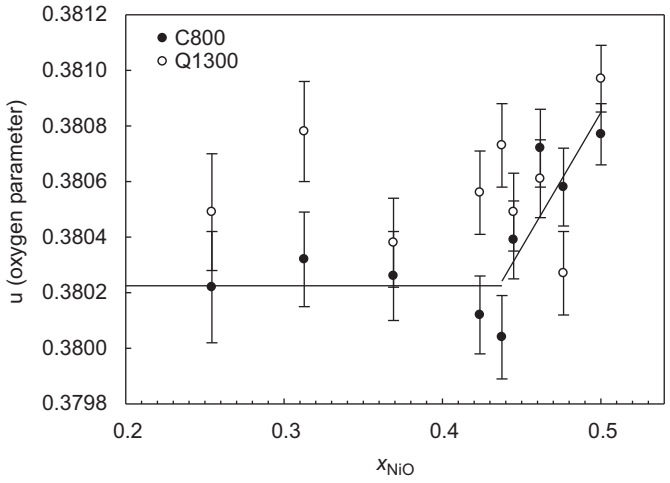

Fig. 5. The oxygen parameter *u* versus the overall composition of the samples.

became gradually transformed to a random spinel at high temperatures, in agreement with previous reports for stoichiometric $NiAl_2O_4$.

Acknowledgment

The work has been carried out with the financial support of VISTA.

References

[1] B. Phillips, J.J. Hutta, I. Warshaw, J. Am. Ceram. Soc. 46 (12) (1963) 579–583.
[2] T. Barry, et al., J. Phase Equilib. 13 (5) (1992) 459–475.
[3] F.A. Elrefaie, W.W. Smeltzer, Oxid. Met. 15 (5–6) (1981) 495–500.
[4] T.F.W. Barth, E. Posnjak, Z. Kristallogr. 82 (1932) 325–341.
[5] H. Schmalzried, Z. Phys. Chem. 28 (1961) 203–219.
[6] R.K. Datta, R. Roy, J. Am. Ceram. Soc. 50 (11) (1967) 578–583.
[7] K. Mocala, A. Navrotsky, J. Am. Ceram. Soc. 72 (5) (1989) 826–832.
[8] H.S.C. O'Neill, W.A. Dollase, C.R. Ross II, Phys. Chem. Miner. 18 (5) (1991) 302–319.
[9] J.N. Roelofsen, R.C. Peterson, M. Raudsepp, Am. Mineral. 77 (5–6) (1992) 522–528.
[10] Y.S. Han, J.B. Li, X.S. Ning, B. Chi, J. Am. Ceram. Soc. 88 (12) (2005) 3455–3457.
[11] M. Munro, J. Am. Ceram. Soc. 80 (8) (1997) 1919–1928.
[12] D.D.I. Halevy, E. Üstündag, A.F. Yue, E.H. Arredondo, J. Hu, M.S. Somayazulu, J. Phys. Condens. Matter 14 (2002) 10511.
[13] H.U. Viertel, F. Seifert, Neues Jahrb. Mineral. Abh. 134 (1979) 167–182.